

F-1. One-Week Ensemble Prediction System at the Japan Meteorological Agency¹

F-1-1. Breeding of Growing Modes

This section describes the Breeding of Growing Modes (BGM; Toth and Kalnay 1993), which had been used in the One-Week Ensemble Prediction System (hereafter referred to as One-Week EPS) at the Japan Meteorological Agency (JMA) until October 2007. The BGM is a method to create initial ensemble perturbations. Multi-independent perturbations can be computed by retaining what is called the breeding cycles, each of which produces a growing mode. The followings are the details of the procedure to create an initial perturbation at an analysis time τ in a breeding cycle. First, a perturbed run is performed from an initial time τ_i to a forecast time τ_j ($\tau_i < \tau_j < \tau$), then the forecast error of the perturbed run is obtained by subtracting an analysis from the perturbed run:

$$\mathbf{e}_i(\tau_j) = \mathbf{x}_i(\tau_j) - \mathbf{a}(\tau_j), \quad (\text{F-1-1})$$

where $\mathbf{e}_i(\tau_j)$ is the forecast error of the perturbed run whose initial and forecast time are τ_i and τ_j , respectively. $\mathbf{x}_i(\tau_j)$ is the perturbed run whose initial and forecast time are also τ_i and τ_j , respectively. $\mathbf{a}(\tau_j)$ is an analysis at τ_j . Second, an initial perturbation at τ_j , $\delta\mathbf{a}(\tau_j)$, is calculated by adjusting the amplitude of the forecast error, $\mathbf{e}_i(\tau_j)$:

$$\delta\mathbf{a}(\tau_j) = C_{amp} \times \frac{\mathbf{e}_i(\tau_j)}{\|\mathbf{e}_i(\tau_j)\|}, \quad (\text{F-1-2})$$

where $\|\cdot\|$ is the norm and C_{amp} is the amplitude of the perturbation. Finally, an initial perturbation at τ , $\delta\mathbf{a}(\tau)$, which is called the bred vector, is generated by conducting both the calculation of the forecast error and the adjustment of the amplitude (hereafter, referred to as scale-down) every perturbed forecast between τ_i and τ .

Utilizing the difference between the non-perturbed run and the perturbed run, \mathbf{d} , instead of the forecast error of the perturbed run as shown in Eq. F-1-1 is also a BGM method called the Self-Breeding of Growing Modes:

$$\mathbf{d}_i(\tau_j) = \mathbf{x}_i(\tau_j) - \mathbf{x}_i^0(\tau_j), \quad (\text{F-1-3})$$

$$\delta\mathbf{a}(\tau_j) = C_{amp} \times \frac{\mathbf{d}_i(\tau_j)}{\|\mathbf{d}_i(\tau_j)\|}, \quad (\text{F-1-4})$$

where $\mathbf{d}_i(\tau_j)$ is the difference between the non-perturbed run and the perturbed run, whose initial and forecast time are τ_i and τ_j , respectively. $\mathbf{x}_i^0(\tau_j)$ represents the non-perturbed run. The Self-Breeding of Growing Modes has a benefit of removing systematic errors of a numerical model from the calculated perturbations because \mathbf{d} is the difference of two numerical integrations.

¹ This Section F-1 is based on Kyouda (2006).

F-1-2. System Configurations of the One-Week EPS

The JMA started an operation of the One-Week EPS in March 2001 following the two-year experimental operation (Hayashi 1997; Kyouda 2000). The BGM method was adopted to build up the EPS until October 2007 when the singular vector (SV) method (e.g. Buizza and Palmer 1995; Barkmeijer et al. 2001) took the place. A model ensemble technique such as a stochastic physics technique (Buizza et al. 1999) has yet to be considered (planned to be implemented as of February 2010). This section describes the configurations of the One-Week EPS during the time when the system used the BGM. Table F-1-1 shows the history of the One-Week EPS from the time of the experimental operation to October 2007. Two major changes occurred: one was the change in the area and the amplitude of the perturbations (Kyouda 2002), which were implemented in February 2002, and the other was the enhancement of the number of breeding cycles from 12 to 25 (Sakai 2006), which was implemented in March 2006. For the numerical model, the lower resolution version of the JMA Global Spectral Model (JMA/GSM, JMA 2007; Iwamura and Kitagawa 2008) was used. Note that the One-Week EPS did not necessarily reflect the latest version of the JMA/GSM. This was because the One-Week EPS had shared the system with the One-Month EPS (Takano 1996), and the One-Month EPS needed to calculate the systematic errors of the new version of the model. Though sharing the same system between them was efficient in terms of saving computer resources, it stopped in March 2006 so that the One-Week EPS could have the benefits of the revised JMA/GSM more quickly. The procedure to make initial perturbations in the One-Week EPS was based on the Self-Breeding of Growing Modes. The way of the scale-down and the amplitude of perturbations were determined as follows:

$$\delta \mathbf{x}(\tau) = C_{amp} \times \frac{\mathbf{P}_{local}(\mathbf{d}(\tau) + \mathbf{r}(\tau))}{\|\mathbf{P}_{local}(\mathbf{d}(\tau) + \mathbf{r}(\tau))\|}, \quad (\text{F-1-5})$$

$$C_{amp} = \frac{0.145 \times \sigma_{Z500}(\tau)}{\|\mathbf{P}_{local} \mathbf{P}_{Z500} \mathbf{d}(\tau)\|} \times \|\mathbf{P}_{local}(\mathbf{d}(\tau) + \mathbf{r}(\tau))\|, \quad (\text{F-1-6})$$

$$\mathbf{r}(\tau) = 0.45 \times \mathbf{P}_q \mathbf{d}(\tau), \quad (\text{F-1-7})$$

where $\delta \mathbf{x}$ is an perturbation, \mathbf{P}_{local} is a local projection operator which makes a vector to zero south of 20° S, and \mathbf{P}_{Z500} and \mathbf{P}_q are also operators which make a vector to zero except the geopotential height at 500 hPa and the specific humidity, respectively. σ_{Z500} , which is a function of days, is the standard deviation of the geopotential height at 500 hPa daily averaged over the North Hemisphere. \mathbf{r} is a vector to amplify the specific humidity component of the perturbation. As Eq. F-1-5 shows, the perturbed area was limited north of 20° S. This was to effectively calculate the initial perturbations which might affect the forecasts around Japan. Another characteristic was the way to calculate C_{amp} , where the geopotential height at 500 hPa was the only factor to determine it. The geopotential height at 500 hPa was also used as a criterion in orthogonalizing the perturbations and in reflecting the distribution of analysis errors into that of the perturbations as will be described later on. C_{amp} was 14.5% of the climatological variance (standard deviation) of the geopotential height at 500 hPa so that the One-Week EPS could secure the proper ensemble spread throughout the forecast period. In

addition, as Eq. F-1-7 shows, the amplitude of the specific humidity component was amplified by 45 %. Moreover, the amplitude of the perturbations was adjusted so that the perturbations would reflect the distribution of analysis errors. This process was performed right after the scale-down at 12 UTC, and the adjusted perturbations were used as initial perturbations for the ensemble forecasts. The purpose of this treatment was to let the BGM, which was just based on the growth rate of perturbations, know the fact that analysis errors vary from place to place (Kyouda 2000). Furthermore, the One-Week EPS installed a process to create the multi-independent perturbations by applying the Gram-Schmidt orthogonalization. This was also conducted right after the scale-down at 12 UTC, but the results were used for the initial perturbations for the next breeding cycles, not for the ensemble forecasts. The aim of the orthogonalization was to make perturbations with the various directions of growing modes, and it is considered that, by performing the orthogonalization, the ensemble spread should become larger. Considering $\delta\mathbf{x}^1$, which is a perturbation coming from the first breeding cycle, as a basis vector, the orthogonalized perturbations, $\delta\mathbf{y}^l$, where l ($l = 2, 3, \dots$) represents the l th breeding cycle, were computed as follows:

$$\mathbf{y}^l = \delta\mathbf{x}^l - a \sum_{i=1}^{l-1} \langle \delta\mathbf{x}^i, \mathbf{P}_{Z500} \delta\mathbf{x}^l \rangle \delta\mathbf{x}^i, \quad (\text{F-1-8})$$

$$\delta\mathbf{y}^l = \frac{\|\mathbf{P}_{Z500} \delta\mathbf{x}^1\|}{\|\mathbf{P}_{Z500} \mathbf{y}^l\|} \mathbf{y}^l, \quad (\text{F-1-9})$$

where \mathbf{P}_{Z500} is an operator which makes a vector to zero except the geopotential height at 500 hPa. a represents the orthogonalization ratio, meaning that $a = 1$ is the Gram-Schmidt orthogonalization. In the One-Week EPS, a is 0.75 in order not to heavily collapse the structure of perturbations with large growth rates.

In November 2007, the One-Week EPS went through another two major revisions; one is the enhancement of the model resolution from TL159L40 to TL319L60, and the other is the change in the method to create the initial perturbations from the BGM to the SV method. The specifications of the One-Week EPS after November 2007 are briefly summarized in F-2 and Yamaguchi et al. (2009a). Using the SV method, the JMA started operating another EPS for typhoon forecasting in February 2008. In F-2, the EPS, the Typhoon EPS, is described.

Table F-1-1. Evolution of the One-Week Ensemble Prediction System until October 2007.

Operational period (Month/Year to Month/Year)	Experimental Operation	Operation		
	Mar./99 to Feb./01	Mar./01 to Feb./02	Feb./02 to Feb./06	Mar./06 to Oct./07
Ensemble size	9	25		51
Initial time	12 UTC			
Forecast range	8 days	9 days		
Numerical model	JMA/GSM			
Resolution	T63L30	T106L40	TL159L40	
Horizontal resolution	1.875°	1.125°		
Vertical levels	30	40		
Initial condition	Global analysis			
Initial perturbations	BGM with breeding cycles of 12 hours			
Breeding cycles	4	12	25	
Perturbed area	North of 20°N			North of 20°S

F-2. Typhoon Ensemble Prediction System at the Japan Meteorological Agency¹

F-2-1. General specifications

The Japan Meteorological Agency (JMA) started operating a new ensemble prediction system (EPS) for typhoon forecasting in February 2008. The Typhoon EPS (hereafter referred to as TEPS) is operated for TCs analyzed by the Regional Specialized Meteorological Center (RSMC) Tokyo - Typhoon Center. It runs up to four times a day starting at 0000, 0600, 1200 and 1800 UTC with a forecast range of 132 hours when the following one of the conditions is satisfied:

1. a TC of tropical storm (TS) intensity (the maximum sustained wind speed of 34 knots to 47 knots near the centre) or higher exists in the RSMC Tokyo - Typhoon Center's area of responsibility (0 – 60N, 100 – 180E);
2. a TC is expected to reach TS intensity or higher in the area within 24 hours;
3. a TC of TS intensity or higher is expected to move into the area within 24 hours.

The NWP model for the TEPS is a global model with a resolution of TL319L60, which is a lower-resolution version of the JMA Global Spectral Model (JMA/GSM) at TL959L60 (Iwamura and Kitagawa, 2008; Nakagawa, 2009). The global analysis for the JMA/GSM at TL959L60, which is based on a four-dimensional variational data assimilation system (4DVAR) (Kadowaki, 2005; JMA, 2007), is interpolated to TL319L60 and used as the initial condition of the TEPS. The ensemble size is set at 11 with one non-perturbed run and ten perturbed runs. The method to create the initial perturbations is the singular vector (SV) method (Buizza, 1994; Molteni et al., 1996; Puri et al., 2001) as used in the One-Week EPS since November 2007. (see Section F-2-2 for details).

F-2-2. Initial perturbations

The TEPS adopts the SV method to generate the initial perturbations. If a perturbation grows linearly, an SV with a large singular value represents a fast-growing perturbation (Lorenz, 1965). In addition, using an SV method enables the computation of perturbations that have a large influence on an arbitrarily chosen domain, which can be associated with the development or movement of TCs when the domain is targeted to the TC's surroundings.

The tangent-linear and adjoint models used for the SV computation come from the JMA global 4DVAR system (Kadowaki, 2005; JMA, 2007), which has been in operation since February 2005. While their resolutions were T159L60 for the 4DVAR as of September 2008, the TEPS uses the lower-resolution version, T63L40. The models consist of full dynamical core and physical processes including vertical diffusion, gravity wave drag, large-scale condensation, long-wave radiation and deep cumulus convection. SVs based on tangent-linear and adjoint models including the full physical processes (the simplified physical processes without the moist processes) are called moist (dry) SVs. The TEPS calculates dry SVs targeting for the mid-latitude area in the RSMC Tokyo - Typhoon Center's area of responsibility, aiming to identify the dynamically most unstable perturbations of the atmosphere, such as the baroclinic instability (Buizza and Palmer, 1995). It also calculates moist SVs targeting for TC surroundings where moist processes are critical (Barkmeijer et al., 2001).

JMA's computing system allows the TEPS to target up to three TCs at a time. If more than

¹ The Section F-2 is based on Yamaguchi et al. (2009a) and Yamaguchi and Komori (2009b).

three TCs are present, three of them are selected in the order of concern of the RSMC Tokyo - Typhoon Center. The targeted area of dry SV calculations is fixed as 20 – 60N, 100 – 180E, and that of moist SV calculations covers a rectangle of 10 degrees in latitude and 20 degrees in longitude with its center at the forecasted TC's central position at a forecast time of 24 hours. The optimization time interval for the SV calculations is 24 hours for both dry and moist SVs. As shown in the following equation (F-2-1), the norm to evaluate the growth rate of dry and moist SVs is based on a total energy norm that includes a specific humidity term (Barkmeijer et al., 2001):

$$\begin{aligned}
(x, \mathbf{E}x) = & \frac{1}{2} \int_0^1 \int_S (\nabla\Delta^{-1}\zeta_x \cdot \nabla\Delta^{-1}\zeta_x + \nabla\Delta^{-1}D_x \cdot \nabla\Delta^{-1}D_x \\
& + g(\Gamma_d - \Gamma)^{-1} \frac{T_x T_x}{T_r} \\
& + w_q \frac{L_c^2}{c_p T_r} q_x q_x) dS \left(\frac{\partial p}{\partial \eta} \right) d\eta \\
& + \frac{1}{2} \int_S \frac{R_d T_r}{P_r} P_x P_x dS,
\end{aligned}
\tag{F-2-1}$$

where ζ_x , D_x , T_x , q_x and P_x are the vorticity, divergence, temperature, specific humidity and surface pressure components of vector x , and \mathbf{E} represents a norm operator. Note that the temperature lapse rate Γ is taken into consideration in an available potential energy term (Lorenz, 1955). c_p is the specific heat of dry air at a constant pressure, L_c is the latent heat of condensation, and R_d is the gas constant for dry air. $T_r = 300$ K is a reference temperature, $P_r = 800$ hPa is a reference pressure, and w_q is a constant ($w_q = 1$ in the TEPS). The representative value of $2/3\Gamma_d$ is used for Γ . In Eq. (F-2-1), the vertical integration of the kinetic energy term and the available potential energy term is limited from the lowest model level to about the 26 the model level (about 100 hPa), and the specific humidity term can be up to the 15th model level (about 500 hPa). Otherwise, as is the case with the study by Barkmeijer et al. (2001), SVs have a shallow vertical structure in the upper troposphere or have a large specific humidity contribution in the upper troposphere where the amount of specific humidity is relatively small. Since such SVs have little influence on TC track forecasts, we set a limit on the vertical integration in Eq. (F-2-1).

Finally, the initial perturbations are generated by linearly combining SVs. Each SV calculation can produce up to ten SVs depending on the operationally allocated calculation time period, which means that up to 40 SVs can be obtained (i.e., 10 dry SVs and 30 moist SVs) for one forecast event. Before determining the binding coefficients, SVs with structures similar those of others are eliminated. When the similarity index (the value of the inner product) of any two SVs is 0.5 or more, one of them is eliminated from the group of SV candidates used to make initial perturbations. After this process, the binding coefficients are determined based on a variance minimum rotation, which makes the spatial distributions of the perturbations widely spread. If no SV is eliminated, we have the same number of independent initial perturbations as the number of SVs computed. For the ten perturbed runs, we select five perturbations randomly from the initial perturbations, and positively and negatively add them to the analysis field. The amplitude of the perturbations is adjusted so that the maximum zonal or meridional wind speed equals 6.0 m/s somewhere in the globe.

Table F-2-1 gives a summary of the specifications. It should be noted that JMA also operates the One-Week Ensemble Prediction System (WMO 2008), which has specifications similar to those of the TEPS but is designed to improve medium-range forecasts. For reference, we add the specifications of the One-Week EPS shown in Table F-2-1.

Table F-2-1. Specifications of the Ensemble Prediction Systems at JMA as of August 2008.

		Typhoon Ensemble Prediction System (TEPS)		One-Week Ensemble Prediction System (WEPS)	
Forecast domain		Global			
Truncation wave number		Spectral triangular truncation at 319 wave numbers with linear Gaussian grid (TL319)			
Horizontal grid, grid spacing		640 x 320, 0.5625 deg. (– 60 km)			
Vertical resolution		60 unevenly spaced hybrid levels (from surface to 0.1 hPa)			
Forecast range		132 hours		216 hours	
Initial time		00, 06, 12, 18 UTC		12 UTC	
Ensemble size		11 members (10 perturbed forecasts and 1 control forecast)		51 members (50 perturbed forecasts and 1 control forecast)	
Perturbation	Perturbation generator	Singular Vector (SV) method			
	Inner model resolution	Spectral triangular truncation at 63 wave numbers (T63), 40 unevenly spaced hybrid levels (from surface to 0.4 hPa)			
	Norm	Moist total energy			
	Perturbed area	Western North Pacific (20 – 60N, 100 – 180E)	3 Typhoons (20 deg. x 10 deg. in the vicinity of each typhoon)	Northern Hemisphere (30 – 90N)	Tropics (20S – 30N)
	Physical process	*Simplified physics	**Full physics	*Simplified physics	**Full physics
	Optimization time interval	24 hours		48 hours	24 hours
	Evolved SV	Not used		Used	

*Simplified physics: initialization, horizontal diffusion, surface turbulent diffusion and vertical turbulent diffusion

**Full physics: the elements of simplified physics plus gravity wave drag, long wave radiation, large-scale condensation and cumulus convection

F-2-3. Case studies

Figure F-2-1 shows examples of forecasts by the TEPS. The upper figures are for typhoon Maria in 2006, initiated at 12 UTC on Aug. 6th, 2006, and the lower figures are for typhoon Chaba in 2004, initiated at 12 UTC on Aug. 28th, 2004. The panels on the left show track forecasts by JMA/GSM (the solid lines) with a best track (the dashed line), while those on the right show all tracks obtained using the TEPS. In the case of Maria, there is a large ensemble spread; some of the ensemble members support the same scenario as JMA/GSM, indicating that Maria is heading for western Japan, while others recurve and head toward eastern Japan. In reality, as the best track shows, Maria recurved and skirted the southern coast of the Kanto region to the east of Japan. It is noteworthy that the TEPS captured the possibility of the best track. From the perspective of disaster prevention or mitigation, it is very important to ascertain all possible scenarios in advance and take measures as needed. The TEPS is expected to enable the capture of such potential track spreads. In contrast to the case with Maria, Chaba shows quite a small ensemble spread, meaning that the confidence of the forecast is relatively high. In fact, the deterministic forecast by JMA/GSM was almost perfect. As in these two cases, we can expect the TEPS to provide track forecast information with high confidence referring to ensemble spreads that could vary by TC and the initial time of forecasting.

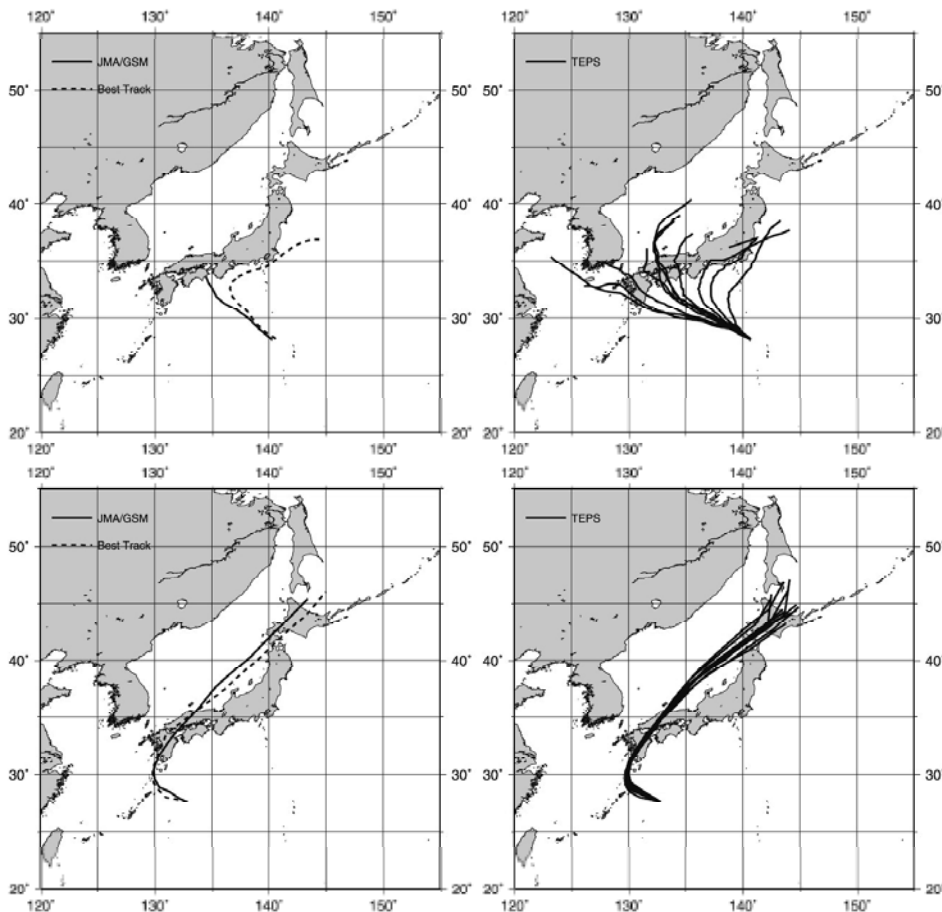


Fig. F-2-1. Example forecasts of the TEPS. The upper figures are for typhoon Maria in 2006, initiated at 12 UTC on Aug. 6th, 2006. The lower figures are for typhoon Chaba in 2004, initiated at 12 UTC on Aug. 28th, 2004. The figures on the left show the track forecast by JMA/GSM (the solid line) with the best track (the dashed line), and those on the right show all track forecasts by the TEPS.

F-2-4. Quasi-operational application

To statistically evaluate the performance of the TEPS, we conducted quasi-operational runs of the TEPS from May to December of 2007. We verified the ensemble mean tracks and the relationship between the position errors of the ensemble mean and the ensemble spreads of tracks. The specifications of the quasi-operational TEPS are different from those of the operational TEPS in several respects. For example, the fields analyzed by the TEPS before November 21st, 2007 (when high resolution JMA/GSM with TL959L60 became operational) come from those of the lower-resolution JMA/GSM with TL319L40. However, we confirmed through one-month period experimentation that these differences in specifications have little influence on the results of the verifications.

a) Ensemble mean track forecast

Figure F-2-2 shows the position errors of the ensemble mean track, which is made by averaging the TC track forecasting by all ensemble members. The verifications are based on the best track data produced by the RSMC Tokyo - Typhoon Center. Both Figs. F-2-2a and 2b are the results of verifying TCs of tropical storm intensity or higher, but Fig. F-2-2b includes the extratropical-transition stages of TC verification. The X-axis represents the forecast time up to five days. The Y-axis on the left gives the position errors (in km) of the control runs, or non-perturbed runs (the thin line), and the ensemble mean (the thick line). The dots correspond to the Y-axis on the right, which represents the number of verification samples. As both Figs. F-2-2a and 2b show, the position errors of the ensemble mean are smaller than those of the control runs in four- and five-day forecasts, although their performance as control runs up to the three-day forecast point is almost identical. The error reduction in five-day forecasts is 40 km (as shown in Fig. F-2-2a), which is equivalent to a gain of about half a day of lead time, given that the position error difference between four-day and five-day forecasts by JMA's global forecasting NWP system was about 100 km in 2007 (see Fig. F-2-3).

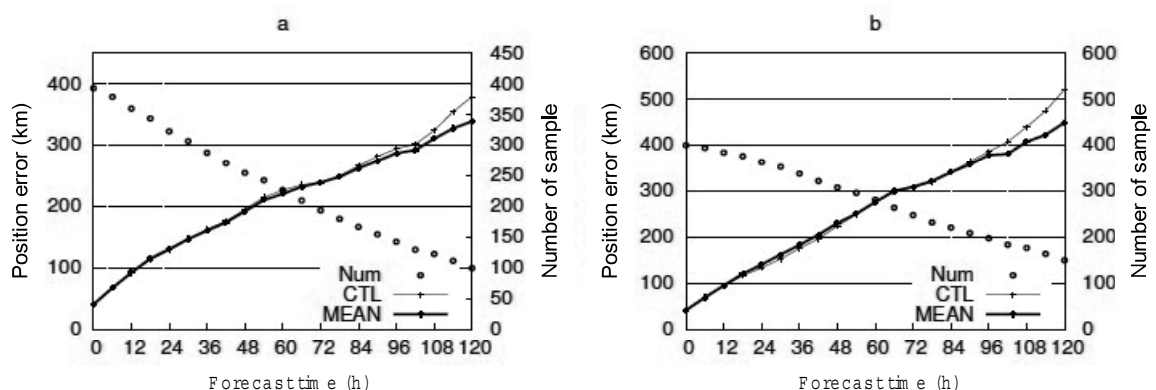


Fig. F-2-2. Position errors (in km) of the ensemble mean (the thick lines) as a function of the forecast time up to 120 hours, compared with those of control runs (the thin lines). The dotted lines correspond to the Y-axis on the right, which represents the number of verification samples. Both a and b are the results of verifying TCs of tropical storm intensity or higher, but b includes the extratropical-transition stages of the TCs verified. The verification period was the quasi-operation period of the TEPS from May to December, 2007.

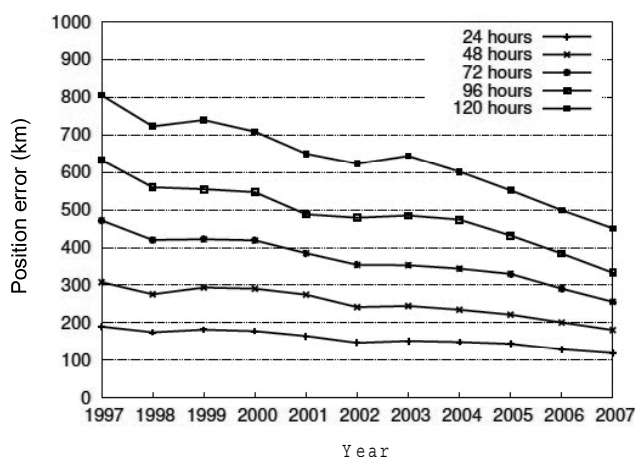


Fig. F-2-3. Time series of the three-year running mean of position errors by JMA’s global forecasting NWP system from 1997 to 2007 (e.g., the verification value for 2007 is the average of those for 2005, 2006 and 2007). Each line represents the errors of 24-, 48-, 72-, 96- and 120-hour forecasts from the bottom up.

b) Confidence information

Figure F-2-4 shows the relationship between the spread of five-day track forecasts and the five-day forecast error of the ensemble mean. The TCs verified are exactly the same as those in Fig. F-2-2b, and each dot gives the verification result of each forecast event. As Fig. F-2-4 shows, there is a strong relationship between the spread and the position error; when the ensemble spreads are relatively small, the position errors of the corresponding forecast events are also small. More importantly, there are no cases with large position errors, which occur when ensemble spreads are relatively large. While Fig. F-2-4’s verification is limited to a forecast time of five days, such a strong relationship can be seen in verifications for other forecast times.

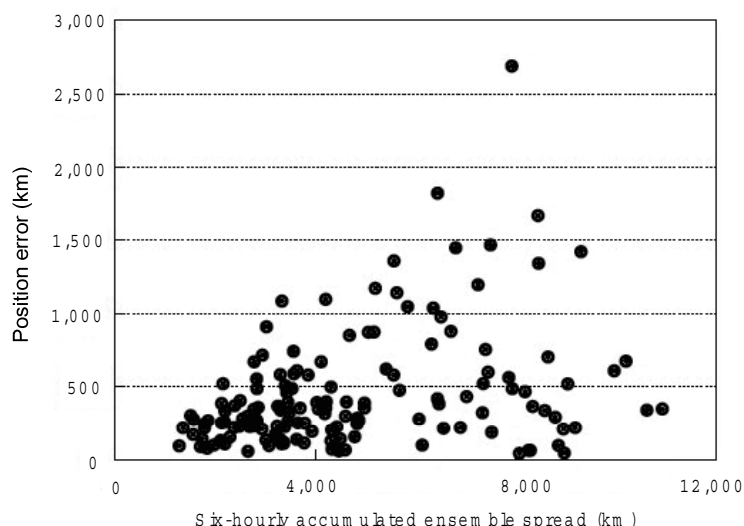


Fig. F-2-4. Relationship between the spread of five-day track forecasts and the five-day forecast error of the ensemble mean. The X-axis represents ensemble spreads (km) accumulated every six hours from the initial time to the five-day stage. The Y-axis represents the position errors (km) of the ensemble mean for the corresponding forecast events. The total number of cases is 149, which is the same as that of the five-day forecasts in Fig. F-2-2b.

Based on this relationship, we classify the confidence level of TC track forecasts (i.e., ensemble mean track forecasts) at each forecast time for each forecast event. A confidence index (A, B or C, representing the categories of the highest, middle-level and lowest confidence, respectively) is allocated, and the frequency of each category is set to 40%, 40% and 20 % respectively. Figure F-2-5 shows that the average position errors in category A are quite small in comparison to those of all track forecasts shown in Fig. F-2-2b. As an example, the position errors of three-day forecasts are about 300 km on average, but become less than 200 km if the samples are limited to cases with small ensemble spreads. Conversely, the average position errors in category C are larger than those of all forecasts.

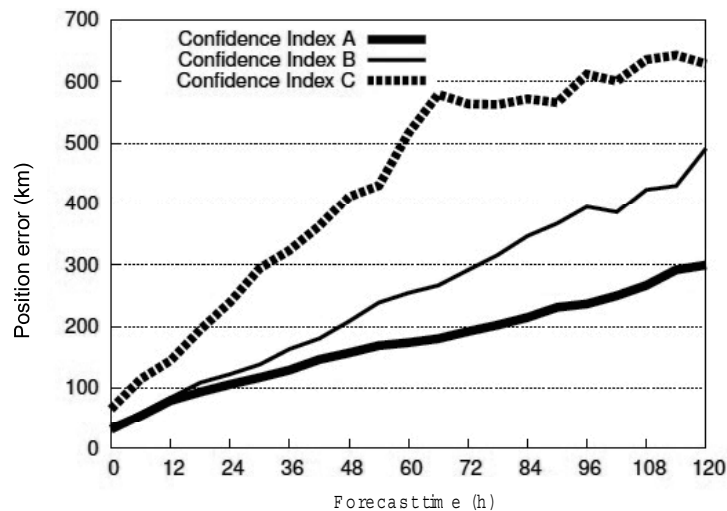


Fig. F-2-5. Verification results of confidence indices on TC track forecasts. Referring to the amount of ensemble spread, a confidence index (A, B or C) is given to ensemble mean track forecasts at each forecast time for each forecast event (A represents the highest level of confidence). The thick line shows the position errors of the ensemble mean for all A cases as a function of the forecast time. The thin and dashed lines represent the B and C cases, respectively.

The reason why the categories are set as 40%, 40% and 20% (rather than 33%, 33% and 33%) is to clearly split the position errors into three lines as in Fig. F-2-5. Figure F-2-6 shows the position error of each three-day forecast by JMA's global NWP system in 2007 with the errors sorted in ascending order. As the figure shows, the frequency distribution of the errors is not uniform, and the rate of cases with a relatively large position error is about 10 to 20% of the total number of events. We therefore set the rate of category C to be smaller than those of categories A and B.

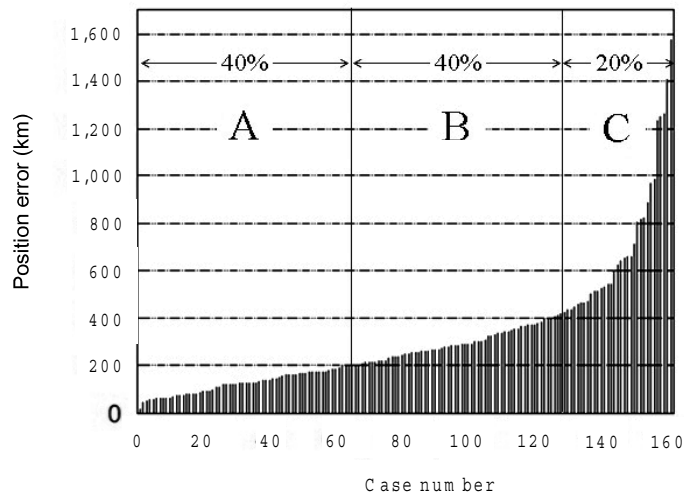


Fig. F-2-6. Position error (km) of each three-day track forecast initiated at 00 UTC by JMA's global forecasting NWP system in 2007. The errors are sorted in ascending order, and the total number of cases is 163.

F-2-5. Summary

The JMA began operation of the new Typhoon EPS in February 2008 with the aim of improving TC track forecasts. The TEPS runs up to four times a day with a forecast range of 132 hours targeting TCs in the western North Pacific, including the South China Sea. It is composed of eleven forecast members derived from the TL319L60 global model. The method of making initial perturbations is based on the SV method.

In order to assess the performance of the TEPS, we conducted quasi-operational forecasts of the system from May to December of 2007. The verification of these quasi-operational runs showed that two benefits can be expected from the TEPS. First, the position errors of deterministic track forecasts will be reduced. Using the ensemble mean obtained a 40-km reduction in five-day track forecasts on average, corresponding to a gain of about half a day of lead time. Second, information on track forecasts' level of confidence can also be obtained. Referring to the ensemble spreads of tracks has enabled the extraction of uncertainty information on track forecasts.

Remaining issues include the question of how to leverage the benefits of the TEPS in operational forecasting. In particular, conveying uncertainty information to public users is challenging, and this point must be kept in mind during the development of related applications.

F-3. NHM-LETKF

F-3-1. Basic concept of LETKF

The ensemble Kalman filter (EnKF), started from Evensen (1994), is an advanced data assimilation method which uses flow-dependent forecast error statistics represented by ensemble prediction. Figure F-3-1 shows a schematic of the basic concept. The ensemble prediction from time $T=t_0$ provides the flow-dependent estimate of the forecast error at $T=t_1$, which is combined with the observation data to generate ensemble initial conditions for the next forecasts; the process is cycled.

If the Gaussian PDF is assumed, the formulas for the optimal combination of the forecast and observation data are given by the following Kalman filter equations (Kalman 1960), or more precisely, extended Kalman filter equations for a nonlinear evolving model M :

1. Forecast equations: $x_i^f = M(x_{i-1}^a)$, $\mathbf{P}_i^f = \mathbf{M}\mathbf{P}_{i-1}^a\mathbf{M}^T$ (F-3-1)

2. Analysis equations: $x_i^a = x_i^f + \mathbf{K}_i(y_i^o - H_i x_i^f)$, $\mathbf{P}_i^a = (\mathbf{I} - \mathbf{K}_i \mathbf{H}_i)\mathbf{P}_i^f$ (F-3-2)

3. Kalman gain equation: $\mathbf{K}_i = \mathbf{P}_i^f \mathbf{H}_i^T (\mathbf{H}_i \mathbf{P}_i^f \mathbf{H}_i^T + \mathbf{R}_i)^{-1}$. (F-3-3)

Here, the notation follows Ide et al. (1994). Due to the high dimension N of numerical weather prediction (NWP) models, typically $N \sim O(10^7)$, the covariance matrix \mathbf{P} is approximated by a limited number m of ensemble members, where typically $m \leq O(100)$:

$$\mathbf{P} \approx \frac{1}{m-1} \delta \mathbf{X} \delta \mathbf{X}^T. \quad (\text{F-3-4})$$

Here, $\delta \mathbf{X}$ is an N -by- m matrix whose columns are ensemble perturbations $\delta x = x - \bar{x}$, where the overbar denotes the ensemble mean. Namely,

$$\delta \mathbf{X} = \begin{pmatrix} \delta x^{(1)} & \dots & \delta x^{(m)} \end{pmatrix}, \quad (\text{F-3-5})$$

where superscripts indicate ensemble indexes. This enables to simplify the Kalman filter equations (F-3-1)-(F-3-3) to constitute the following EnKF equations:

1. Forecast equations: $x_i^{f(k)} = M(x_{i-1}^{a(k)})$, $k = 1, \dots, m$, (F-3-6)

2. Analysis equations: $\bar{x}_i^a = \bar{x}_i^f + \mathbf{K}_i(y_i^o - \overline{H_i x_i^f})$, $\mathbf{P}_i^a = (\mathbf{I} - \mathbf{K}_i \mathbf{H}_i)\mathbf{P}_i^f$, (F-3-7)

3. Kalman gain equation: $\mathbf{K}_i = \delta \mathbf{X}_i^f \delta \mathbf{Y}_i^T (\delta \mathbf{Y}_i \delta \mathbf{Y}_i^T + (m-1)\mathbf{R}_i)^{-1}$. (F-3-8)

Here, $\delta \mathbf{Y} = \mathbf{H} \delta \mathbf{X}$ is introduced. It is usually difficult to solve the second analysis equation for the

covariance matrix, or equivalently, to update the ensemble perturbations. Several algorithms have been proposed, such as ensemble adjustment Kalman filter (EAKF, Anderson 2001), ensemble transform Kalman filter (ETKF, Bishop et al. 2001), and serial ensemble square root filter (serial EnSRF, Whitaker and Hamill 2002). The local ensemble transform Kalman filter (LETKF, Hunt et al. 2007) follows the ETKF approach for solving this. Namely, the transform matrix \mathbf{T} will be applied for updating ensemble perturbations:

$$\delta\mathbf{X}^a = \delta\mathbf{X}^f \mathbf{T}, \quad (\text{F-3-9})$$

which must satisfy (F-3-7). To be more specific, Eq. (F-3-4) is rewritten as

$$\mathbf{P}^f \approx \frac{\delta\mathbf{X}^f (\delta\mathbf{X}^f)^T}{m-1} = \delta\mathbf{X}^f \tilde{\mathbf{P}}^f (\delta\mathbf{X}^f)^T. \quad (\text{F-3-10})$$

Here, $\tilde{\mathbf{P}}^f = \frac{\mathbf{I}}{m-1}$ is considered to be the forecast error covariance matrix in the space spanned by forecast ensemble perturbations, or the “tilde space”. Note that the tilde space has only m dimensions. The analysis error covariance matrix in the tilde space turns out to be

$$\tilde{\mathbf{P}}^a = [(m-1)\mathbf{I} / \rho + (\delta\mathbf{Y})^T \mathbf{R}^{-1} \delta\mathbf{Y}]^{-1} = \mathbf{U} \mathbf{D}^{-1} \mathbf{U}^T, \quad (\text{F-3-11})$$

where ρ is the covariance inflation factor. Here, \mathbf{U} and \mathbf{D} are obtained by the following eigenvalue decomposition:

$$(m-1)\mathbf{I} / \rho + (\delta\mathbf{Y})^T \mathbf{R}^{-1} \delta\mathbf{Y} = \mathbf{U} \mathbf{D} \mathbf{U}^T. \quad (\text{F-3-12})$$

Finally, the analysis equations for LETKF are written as

$$\bar{x}^a = \bar{x}^f + \delta\mathbf{X}^f \tilde{\mathbf{P}}^a (\delta\mathbf{Y})^T \mathbf{R}^{-1} (y^o - \overline{H(x^f)}), \quad (\text{F-3-13})$$

$$\delta\mathbf{X}^a = \delta\mathbf{X}^f [(m-1)\tilde{\mathbf{P}}^a]^{1/2} = \delta\mathbf{X}^f \sqrt{m-1} \mathbf{U} \mathbf{D}^{-1/2} \mathbf{U}^T. \quad (\text{F-3-14})$$

Combining (F-3-13) and (F-3-14), we get the more efficient single analysis equation for LETKF:

$$\mathbf{X}^a = \bar{x}^f \mathbf{e} + \delta\mathbf{X}^f \left(\tilde{\mathbf{P}}^a (\delta\mathbf{Y})^T \mathbf{R}^{-1} (y^o - \overline{H(x^f)}) \mathbf{e} + \sqrt{m-1} \mathbf{U} \mathbf{D}^{-1/2} \mathbf{U}^T \right). \quad (\text{F-3-15})$$

Here, \mathbf{e} is an m -dimensional row vector (1, ..., 1).

An important advantage of LETKF is its parallel efficiency. LETKF is different from ETKF in

the sense that it treats each grid point independently. Namely, we solve Eq. (F-3-15) for each grid point separately; the idea is based on the local ensemble Kalman filter (LEKF, Ott et al. 2004). The error covariance is localized when it chooses a subset of observation data to be assimilated at each grid point separately. For smoother localization, the observation error standard deviation is inflated by a smooth weighting function according to the distance from the analyzed grid point. This “observation localization” was proposed by Hunt (2005) and tested by Miyoshi (2005) successfully.

Based on the test of LETKF with a low-resolution global primitive-equation model by Miyoshi (2005), Miyoshi and Yamane (2007) developed and tested the LETKF with AFES (AGCM for the Earth Simulator) with a massively parallel computing environment. Miyoshi and Aranami (2006) applied the AFES-LETKF system to NHM; the details of the application to NHM are described in the following section.

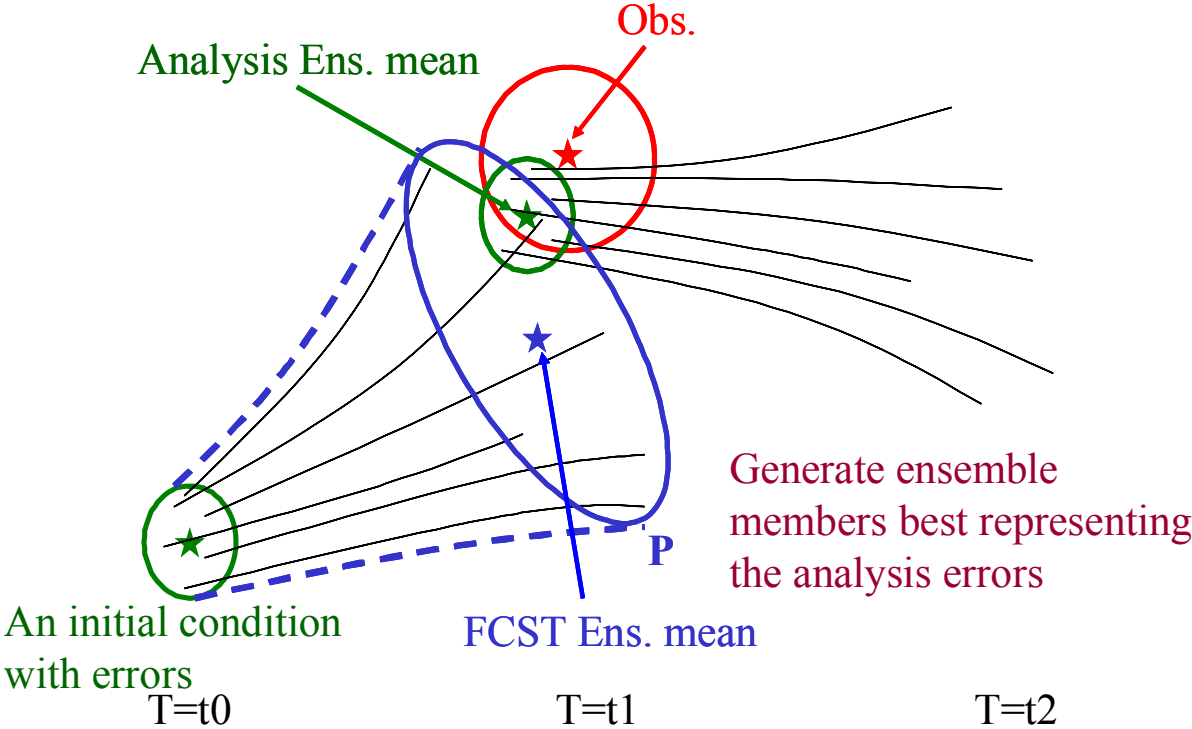


Fig. F-3-1. A schematic showing the basic concept of EnKF. Ellipses indicate contours of equal probability. Black lines indicate trajectories of ensemble prediction.

F-3-2. Practical application to NHM

Miyoshi and Aranami (2006) applied the LETKF system to NHM by taking the most advantage of the model-independent nature of the LETKF. The interfaces of Miyoshi and Yamane's (2007) LETKF based on AFES (AGCM for the Earth Simulator, Ohfuchi et al. 2004) were modified to account for the difference between NHM and AFES (Table F-3-1); in particular, the modifications are adding variables and modifying the boundary treatments. The version of the AFES-LETKF is an earlier one before removing the local patches (Miyoshi et al. 2007), which is identical to what Miyoshi and Yamane (2007) used.

NHM contains more prognostic variables than AFES. The prognostic variables of AFES, a typical AGCM, are composed of horizontal wind components (u , v), temperature (T), water vapor (q_v), liquid water content (q_l), and surface pressure (p_s). In addition, NHM, a typical nonhydrostatic mesoscale model, includes vertical wind component (w), three-dimensional atmospheric pressure (p), and various types of water quantities such as rain (q_r), cloud liquid water (q_c), cloud ice (q_{ci}), snow (q_s), and graupel (q_g). In addition to the prognostic variables, accumulated rain amount is added for assimilating surface rain data. It is important to note that 1-km resolution surface rain accumulation data are available in Japan, which is known as the Radar-AMEDAS (R/A) data, analyzed by combining the radar reflectivity and the surface rain gauge network known as AMEDAS as dense as 20-km mesh over Japan islands. The additional variables are simply added to the LETKF system.

The other major modification is about the forecast domain. We no longer have to consider the cyclic lateral boundary, which makes the system significantly simpler. The local patch near the lateral boundary has smaller size as in the local patch B in Fig. F-3-2. We simply remove the grid points out of the forecast model domain, so that the local patches near the lateral boundary have fewer grid points. The treatment is essentially identical to what has already been implemented for the vertical localization. The vertical local patch is simply shrunk when it exceeds the top/bottom levels. By contrast, no lateral boundary exists in global models, where all local patches have essentially the same size in the horizontal. The later upgrades of removing local patches by Fujita (2007, personal communication), similarly to the later version of AFES-LETKF by Miyoshi et al. (2007), do not require such special treatment to the lateral boundary. This is considered to be an advantage of removing local patches.

The NHM-LETKF with the above modifications from the AFES-LETKF system has been successfully tested by Miyoshi and Aranami (2006). The results are not repeated here, but we would like to discuss some additional aspects. One is the error covariance about the water-related variables. The NHM-LETKF has been developed simply by adding variables without much attention about the inter-variable error covariance localization. If no significant error correlation is expected between variables, the error covariance would likely be affected by sampling noise due to the limited ensemble size. Such error covariance should be zeroed out by localization. This may likely be the case for the water-related variables. More careful studies about the error correlations of water-related variables are desired. If it turns out that it would be better to zero out such error covariance, we would not need to analyze the water-related variables other than q_v unless there are direct observations of water-related quantities such as cloud particles. This makes the system much simpler by reducing analyzing variables by about half. Another aspect is the role of the vertical wind component w , which may mostly be a dependent variable in the dynamics. That is, if we analyze u and v adequately, it spins up

w easily; on the contrary, correct analysis of w may not help much to improve the forecast. A similar discussion may be true to the three-dimensional atmospheric pressure. The difference from hydrostatic balance may produce high-frequency noise, which may be better reduced. If these are all true, we may not need to analyze the additional variables such as w , q (other than q_v) and p (except for surface pressure), so that we could keep essentially the same system as the AFES-LETKF, except for the treatment of the lateral boundary. This enables to share most parts of the LETKF system for both global and regional NWP, and to benefit low-cost development and maintenance. The above discussion may not be true if direct observations of water quantities are important for storm-scale NWP with a very fine resolution, e.g., $O(\sim 1 \text{ km})$ or finer.

Table F-3-1. Major differences between AFES and NHM to be considered in implementing the LETKF.

	AFES	NHM
Forecast domain	Global with cyclic boundary	Regional with fixed boundary
Prognostic variables	u, v, T, q_v, q_l, p_s	$u, v, w, T, p, q_v, q_r, q_c, q_{ci}, q_s, q_g$

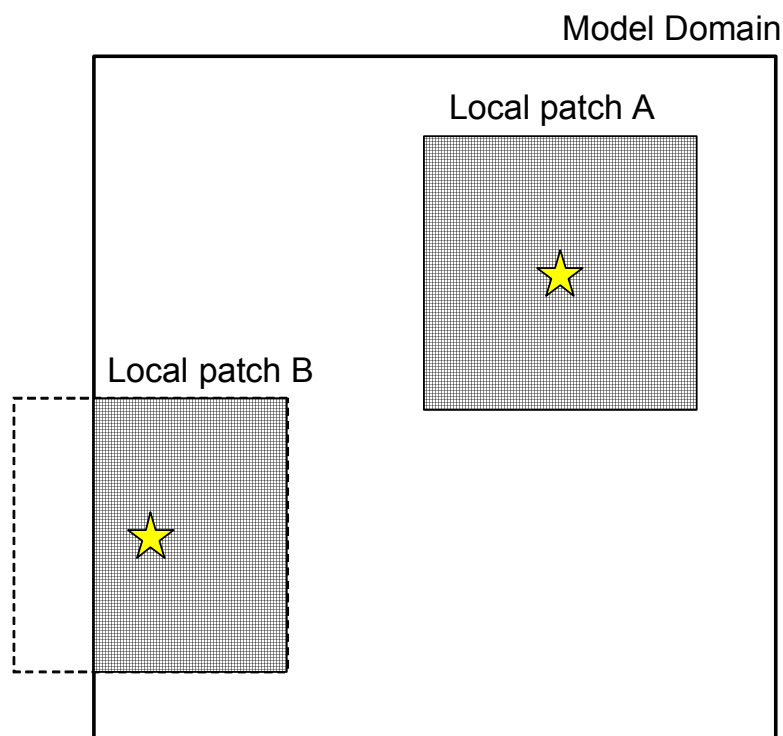


Fig. F-3-2. Schematic showing how to treat local patches near the boundary of the forecast model domain. The local patches A and B indicate examples without and with affected by the boundary, respectively. The stars indicate the center points of the local patches A and B.

F-4. Surface process

The role of surface process is to give the lower boundary conditions to atmosphere, which are represented as surface fluxes of momentum, heat and moisture from the surface to atmosphere. It is considerably important to simulate accurate surface fluxes because not only they affect the prediction of wind and temperature near the surface, but also they drive turbulence in boundary layer which develops and decays well-mixed layer at the lower atmosphere. In this section, the details of the surface flux scheme and the method for predicting soil moisture to evaluate evaporation efficiency at surface are described. While the soil temperature including the surface is predicted in the model, the method has been mentioned in Saito et al. (2001).

F-4-1. Surface flux scheme

In NHM, the surface fluxes are evaluated by the bulk method, in which surface fluxes of momentum $(\overline{w'u'})_0$, heat $(\overline{w'\theta'})_0$ and moisture $(\overline{w'q_v'})_0$ are given as,

$$(\overline{w'u'})_0 = -C_m u_a^2, \quad (\text{F-4-1})$$

$$(\overline{w'\theta'})_0 = -C_h u_a (\theta_a - \theta_s), \quad (\text{F-4-2})$$

$$(\overline{w'q_v'})_0 = -C_h u_a (q_{va} - q_{vs}), \quad (\text{F-4-3})$$

where suffixes a and s denote the lowest level of atmosphere and surface, respectively. The coefficients C_m , C_h are called bulk coefficients, and the main role of surface flux scheme is to determine these coefficients¹.

In NHM employed in the B08FDP/RDP experiment, the bulk coefficients C_m and C_h are determined on the basis of the Monin-Obukhov similarity theory as

$$C_m = \frac{k^2}{\Phi_m(z, L)^2}, \quad (\text{F-4-4})$$

$$C_h = \frac{k^2}{\Phi_m(z, L)\Phi_h(z, L)}, \quad (\text{F-4-5})$$

where

$$\Phi_m(z, L) = \ln \frac{z}{z_{0m}} - \psi_m(\zeta) + \psi_m(\zeta_{0m}), \quad (\text{F-4-6})$$

$$\Phi_h(z, L) = \ln \frac{z}{z_{0h}} - \psi_h(\zeta) + \psi_h(\zeta_{0h}), \quad (\text{F-4-7})$$

¹Although C_h and the coefficient for $\overline{w'q_v'}$ could have different values, the surface scheme in NHM assumes them equal.

$$\zeta \equiv \frac{z}{L}, \quad \zeta_{0m} \equiv \frac{z_{0m}}{L}, \quad \zeta_{0h} \equiv \frac{z_{0h}}{L}, \quad (\text{F-4-8})$$

and $k = 0.4$ is the von Kálmán constant. ψ_m and ψ_h are called the integrated stability functions and given based on Beljaars and Holtslag (1991) as

$$\psi_m(\zeta) = \begin{cases} -b \left(\zeta - \frac{c}{d} \right) \exp(-d\zeta) - a\zeta - \frac{bc}{d} & (\zeta \geq 0) \\ \frac{\pi}{2} - 2 \tan^{-1} x + \ln \frac{(1+x)^2(1+x^2)}{8} & (\zeta < 0) \end{cases}, \quad (\text{F-4-9})$$

$$\psi_h(\zeta) = \begin{cases} -b \left(\zeta - \frac{c}{d} \right) \exp(-d\zeta) - \left(1 + \frac{2}{3} a\zeta \right)^{\frac{3}{2}} - \frac{bc}{d} + 1 & (\zeta \geq 0) \\ 2 \ln \frac{1+x^2}{2} & (\zeta < 0) \end{cases}, \quad (\text{F-4-10})$$

where

$$a = 1, \quad b = \frac{2}{3}, \quad c = 5, \quad d = 0.35, \quad x = (1 - 16\zeta)^{\frac{1}{4}}.$$

L is the Monin-Obukhov length defined with friction velocity $u_* = [-(\overline{u'w'})_0]^{1/2}$ and friction virtual potential temperature $\theta_{v*} = -(\overline{w'\theta'_v})_0 / u_*$ by

$$L = \frac{1}{k} \frac{1}{\frac{g}{\theta_v} \theta_{v*}} \frac{u_*^2}{\theta_{v*}}. \quad (\text{F-4-11})$$

L can be obtained by solving the following equation numerically,

$$\text{Ri}_B = \frac{z}{L} \frac{\Phi_h(z, L)}{\Phi_m(z, L)^2}, \quad (\text{F-4-12})$$

where Ri_B is the bulk Richardson number, defined by

$$\text{Ri}_B = \frac{gz}{\frac{\theta_{va} + \theta_{vs}}{2}} \frac{\theta_{va} - \theta_{vs}}{u_a^2}. \quad (\text{F-4-13})$$

F-4-2. Evaporation efficiency at surface

In Eq. (F-4-3) providing moisture flux $\overline{w'q'_v}$, specific humidity of air in soil near surface, q_s , is required, although it is very difficult to measure. Instead of q_s , we write (F-4-3) with saturated specific humidity at surface, $q_{\text{sat}}(T_s)$, determined only by surface temperature T_s as,

$$\overline{w'q'_v} = -C_q \beta u_a [q_{va} - q_{\text{sat}}(T_s)], \quad (\text{F-4-14})$$

where β is efficiency of evaporation from surface to atmosphere varying between 0 and 1. With (F-4-3) and (F-4-14), q_s can be expressed as,

$$q_s = (1 - \beta)q_{va} + \beta q_{sat}, \quad (\text{F-4-15})$$

which means that q_s is weighted average of q_{va} and q_{sat} with β being a weight factor. As it is significantly related to soil moisture, β is represented with w_g , the volume fraction of soil moisture over a depth of d_1 to which the diurnal cycle of soil moisture can be observed, in the form

$$\beta = \begin{cases} w_g / 0.3 & (w_g \leq 0.3) \\ 1 & (w_g > 0.3) \end{cases}. \quad (\text{F-4-16})$$

NHM has two options to determine w_g : the mode in which w_g is kept its climatic value during forecast period, and the other one in which w_g is predicted by the force-restore method based on Deardorff (1978).

In the force-restore method, the prognostic variables w_g and w_2 , the volume fraction of soil moisture averaged over a depth of d_2 below which the moisture flux can be neglected, are ruled by the following equations:

$$\frac{\partial w_g}{\partial t} = -\frac{w_g - w_2}{\tau_g} + F_g, \quad (\text{F-4-17})$$

$$\frac{\partial w_2}{\partial t} = F_2, \quad (\text{F-4-18})$$

where F_g and F_2 are forcing terms for w_g and w_2 , respectively. These equations mean that w_g is changing to w_2 with a time constant τ_g as (F-4-19) can be solved under the assumptions $F_g = F_2 = 0$ as

$$w_g(t) = w_2 + (w_g(0) - w_2) \exp[-t / \tau_g]. \quad (\text{F-4-19})$$

Referring to Deardorff (1978), some constants and forcing terms appeared in the equations are given as following:

$$\tau_g = C_2 \times 86400, \quad (\text{F-4-20})$$

$$F_g = -C_1 \frac{E - P}{\rho_w d_1}, \quad (\text{F-4-21})$$

$$F_2 = -\frac{E - P}{\rho_w d_2}, \quad (\text{F-4-22})$$

$$d_1 = 0.1, \quad (\text{F-4-23})$$

$$d_2 = 0.5, \quad (\text{F-4-24})$$

with constants C_1 and C_2 ,

$$C_1 = \begin{cases} 0.5 & \left(\frac{w_g}{w_{\max}} \geq 0.75 \right) \\ 14 - 22.5 \left(\frac{w_g}{w_{\max}} - 0.15 \right) & \left(0.15 < \frac{w_g}{w_{\max}} \leq 0.75 \right), \\ 14 & \left(\frac{w_g}{w_{\max}} \leq 0.15 \right) \end{cases}, \quad (\text{F-4-25})$$

$$C_2 = 0.9. \quad (\text{F-4-26})$$

where w_{\max} denotes the maximum value of w_g and w_2 and is set to 0.4. If w_g exceeds w_{\max} , w_g is forced to be w_{\max} , which implies that runoff of precipitation is occurred.

With the parameters given above, temporary changing rates of the prognostic variables tend to be too large. In order to restrict the prognostic variables within appropriate range of values, w_g and w_2 are allowed to vary only between $F_{\min} w_{\text{ini}}$ and $F_{\max} w_{\text{ini}}$, where w_{ini} is the initial value of w_g and w_2 , $F_{\min} (< 1)$ and $F_{\max} (> 1)$ are factors to implement the limitation for w_g and w_2 .

F-5. Turbulent process

In the atmosphere, turbulence of various scales can be observed, and attributes to transport of momentum, heat and moisture. In particular, the vertical transport is significantly important to represent developing and decaying homogeneously mixed layer and generating clouds capping boundary layer.

In most of turbulent models, the vertical flux of certain physical quantity χ , which is denoted as $\overline{w'\chi'}$, is parameterized as

$$\overline{w'\chi'} = -K_\chi \frac{\partial \overline{\chi}}{\partial z} + \Gamma_\chi. \quad (\text{F-5-1})$$

It is the main role of a boundary layer scheme (or a turbulence scheme) in models for the numerical weather prediction (NWP) to evaluate the diffusion coefficient K_χ , and the non-gradient term Γ_χ in Eq. (F-5-1).

There are several models suggested to determine the fluxes. One of those is based on stability functions, often combined with non-local parameterizations (e.g. Lock et al. (2000)). In this kind of schemes, K_χ and Γ_χ are given as functions depending on local stability such as the Richardson number calculated from values on grids, and non-local quantity such as height of boundary layer, cloud base and cloud height. It is classified as the first order model because the fluxes (i.e. the second order moments) are parameterized with values on grids. Other group of turbulence models is based on the relation between the diffusion coefficients and turbulent kinetic energy (TKE) E suggested by Kolmogorov (1942) and Prandtl (1945) independently:

$$K_\chi = CE^{\frac{1}{2}}\ell, \quad (\text{F-5-2})$$

with scale length of the turbulence ℓ . It can be regarded as an analogy of molecular diffusion where the diffusion coefficient K is provided using the mean free path ℓ and scale velocity v_t by

$$K \sim v_t \ell, \quad (\text{F-5-3})$$

since scale velocity of turbulence is well represented by $E^{\frac{1}{2}}$.

In NHM, the latter type of schemes has been used since its initial development. NHM was originally being developed as a cloud resolving model with very high resolutions, and the eddy viscosity model was implemented as a turbulence scheme to represent mixing in boundary layer. As the original purpose of the eddy viscosity model is to represent subgrid turbulence which cannot be resolved on grids, it should work well in very high resolution models. On the other hand, it was revealed that turbulence targeted by the eddy viscosity model was so small compared with the resolution of coarser models such as the operational model that it was not enough to represent vertical transports in boundary layer, while it had been used in the operational mesoscale model with the 10km or 5km horizontal resolution until May 2007.

Instead of the eddy viscosity model, in the current operational MSM as well as the model used in B08RDP, the improved Mellor-Yamada model (Nakanishi, 2001; Nakanishi and Niino, 2004, 2006) (hereafter, MYNN) has been employed (Hara, 2007; Saito et al., 2007). The source code of the main part of the scheme was provided by Nakanishi and the scheme was implemented to NHM with some modifications.

In this section, review of the turbulence schemes in NHM, mainly the improved Mellor-Yamada

scheme, will be made.

F-5-1. Eddy viscosity model

Before going to the current scheme, the former eddy viscosity model is briefly reviewed to make it easy to understand what turbulence scheme is doing in the model with the simpler model and see differences between the former and current schemes.

Deardorff (1980) adopted the eddy-viscosity model, which is also the first order model, with diffusion coefficients derived by TKE as Eq. (F-5-2) for their very high resolution model to parameterize subgrid turbulence. In the model, the second order moments are parameterized by

$$\overline{u_i' u_j'} = -K_m \left(\frac{\partial \bar{u}_i}{\partial x_j} + \frac{\partial \bar{u}_j}{\partial x_i} \right) + \frac{2}{3} E \delta_{ij},$$

$$\overline{u_i' c'} = -K_h \frac{\partial \bar{c}}{\partial x_i}$$

where c denotes any scalar quantities, and the scale length, also known as mixing length, is given by

$$\ell = \begin{cases} 0.76 E^{1/2} / N & (N^2 \geq 0) \\ \Delta z & (N^2 < 0) \end{cases} \quad (\text{F-5-4})$$

with the Brunt-Vaisala frequency N and a grid interval Δz . While the scheme was developed for very high resolution models where large eddies are directly resolved and subgrid ones should be parameterized, Sun and Chang (1986) tried to introduce the same scheme to their coarser GCM with modification of the mixing length depending on the height of mixed layer, which implies introduction of non-locality. The non-local like mixing length was also implemented to NHM and had been employed in the operational meso scale model (MSM) (the horizontal resolution of which is 10km until February 2006, 5km after then) at JMA until May 2007.

Due to its simplicity, the eddy viscosity model had been widely used in numerical models. Transport by small turbulence can be significantly explained by the down gradient method and that is the reason why the eddy viscosity model has been used to parameterize subgrid turbulence. However, it was pointed out that the local K approach like the eddy viscosity model often underestimates transport in boundary layer on coarser resolution models such as operational models and climate models (Holtslag and Boville, 1993). In coarser models, turbulent transport which can not be described with the eddy viscosity model should be parameterized as well.

Furthermore, fully vertically uniform layer often observed in the real world cannot be realized mathematically only with the down gradient formulation when fluxes are being provided from boundaries such as surface and the top of boundary layer. In order to keep boundary layer as uniform as possible with being provided momentum, heat and moisture fluxes from the boundaries, vertical gradient is required for them to be transported into the boundary layer under the down gradient approach. If fully mixed layer were realized with the down gradient approach, no more transportation could be occurred and fluxes given from boundaries could not be transported into the mixed layer, resulting in accumulation near the boundaries.

To overcome the issue, the non-local approach was introduced (Troen and Mahrt, 1986; Holtslag and Moeng, 1991), in which the flux $\overline{w'c'}$ is parameterized as

$$\overline{w'c'} = -K_h \left(\frac{\partial \bar{c}}{\partial z} - \gamma_c \right). \quad (\text{F-5-5})$$

Here, γ_c depends on non-local quantities such as boundary layer height, velocity scales and surface flux, and can be regarded as non-gradient terms that can drive turbulent transport even when fully mixed layer is achieved.

F-5-2. Mellor-Yamada model

The Mellor-Yamada model (Mellor and Yamada, 1974; 1982) (hereafter, MY) is the second order closure model which assumes that the third order moments can be given with the second order ones. The full model (called “Level 4”) requires too much computational costs because all the second order moments are prognostic variables. In order to reduce the computational costs to run, some terms appeared in the prognostic equations are neglected in terms of the order of anisotropy. In the model called “Level 3” with the boundary layer approximation in which horizontal derivatives are ignored, just only four prognostic variables are remained:

$$\frac{Dq^2}{Dt} = -2 \left(\overline{u'w'} \frac{\partial \bar{u}}{\partial z} + \overline{v'w'} \frac{\partial \bar{v}}{\partial z} \right) + 2 \frac{g}{\theta_v} \overline{w'\theta_v'} - 2\varepsilon + \text{dif}.q^2, \quad (\text{F-5-6})$$

$$\frac{D\overline{\theta_1'^2}}{Dt} = -2\overline{w'\theta_1'} \frac{\partial \bar{\theta}_1}{\partial z} - 2\varepsilon_\theta + \text{dif}.\overline{\theta_1'^2}, \quad (\text{F-5-7})$$

$$\frac{D\overline{q_w'^2}}{Dt} = -2\overline{w'q_w'} \frac{\partial \bar{q}_w}{\partial z} - 2\varepsilon_q + \text{dif}.\overline{q_w'^2}, \quad (\text{F-5-8})$$

$$\frac{D\overline{\theta_1'q_w'}}{Dt} = -\overline{w'\theta_1'} \frac{\partial \bar{q}_w}{\partial z} - \overline{w'q_w'} \frac{\partial \bar{\theta}_1}{\partial z} - 2\varepsilon_{\theta q} + \text{dif}.\overline{\theta_1'q_w'}, \quad (\text{F-5-9})$$

where

$$q^2 = 2\text{TKE} = \frac{1}{2} \left(\overline{u'^2} + \overline{v'^2} + \overline{w'^2} \right), \quad (\text{F-5-10})$$

$$\theta_1 = \theta - \frac{L}{C_p} \frac{\theta}{T} q_1, \quad (\text{F-5-11})$$

$$q_w = q_v + q_1, \quad (\text{F-5-12})$$

$$q_1 = q_c + q_{ci}, \quad (\text{F-5-13})$$

with the assumptions that the vertical derivative of the third order moments can reduce to diffusion terms ($\text{dif}.X$ denotes a diffusion term on X). The dissipation terms ε_X appeared in the equations

are parameterized on the basis of the Kolmogorov's local isotropy assumption as

$$\begin{aligned}\varepsilon &= \frac{q}{B_1 \ell} q^2, \\ \varepsilon_\theta &= \frac{q}{B_2 \ell} \overline{\theta_1'^2}, \quad \varepsilon_q = \frac{q}{B_2 \ell} \overline{q_w'^2}, \quad \varepsilon_{\theta q} = \frac{q}{B_2 \ell} \overline{q_w' \theta_1'},\end{aligned}\tag{F-5-14}$$

with the closure constants B_1 , B_2 and the mixing length ℓ . The original MY gives the mixing length as

$$\frac{1}{\ell} = \frac{1}{L_S} + \frac{1}{L_T},\tag{F-5-15}$$

$$L_S = kz, \quad L_T = \alpha \frac{\int_0^\infty qz \, dz}{\int_0^\infty q \, dz},\tag{F-5-16}$$

with an empirical constant α and the von Karman constant k . Because the contribution from L_S is dominant near surface where z is small, it is smoothly connected with the length scale in the neutral surface layer kz . On the other hand, L_T is reflected by vertical distribution of TKE. When large TKE exists at the upper layer, L_T can be large.

The other non-zero second moments become diagnostic variables because time derivatives of them are regarded as higher order terms and eliminated through the simplification from Level 4 to Level 3. After solving the algebraic simultaneous equations on the diagnostic variables, the fluxes in the Level 3 model are represented as the following:

$$\overline{w'u'} = -q\ell(S_{M2.5} + S_M') \frac{\partial \bar{u}}{\partial z},\tag{F-5-17}$$

$$\overline{w'v'} = -q\ell(S_{M2.5} + S_M') \frac{\partial \bar{v}}{\partial z},\tag{F-5-18}$$

$$\overline{w'\theta_1'} = -q\ell(S_{H2.5} + S_H') \frac{\partial \bar{\theta}_1}{\partial z} = -q\ell \left(S_{H2.5} \frac{\partial \bar{\theta}_1}{\partial z} + \Gamma_\theta \right),\tag{F-5-19}$$

$$\overline{w'q_w'} = -q\ell(S_{H2.5} + S_H') \frac{\partial \bar{q}_w}{\partial z} = -q\ell \left(S_{H2.5} \frac{\partial \bar{q}_w}{\partial z} + \Gamma_q \right).\tag{F-5-20}$$

Here, $S_{M2.5}$ and $S_{H2.5}$ are non-dimensional diffusion coefficients depending on the flux Richardson number defined R_f by

$$R_f = -\frac{G_H}{G_M},\tag{F-5-21}$$

$$G_M = \frac{\ell^2}{q^2} \left[\left(\frac{\partial \bar{u}}{\partial z} \right)^2 + \left(\frac{\partial \bar{v}}{\partial z} \right)^2 \right], \quad (\text{F-5-22})$$

$$G_H = -\frac{\ell^2}{q^2} \frac{g}{\theta_v} \left(\beta_\theta \frac{\partial \bar{\theta}_1}{\partial z} + \beta_q \frac{\partial \bar{q}_w}{\partial z} \right), \quad (\text{F-5-23})$$

and S_M and S_H are corrections induced in the Level 3 model.

β_θ and β_q appeared in G_H are parameters associated with buoyancy flux $(g/\theta_v) \overline{w'\theta_v'}$ such as

$$\overline{w'\theta_v'} = \beta_\theta \overline{w'\theta_1'} + \beta_q \overline{w'q_w'}. \quad (\text{F-5-24})$$

The two parameters are evaluated considering subgrid partial condensation, the details of which will be described later. The buoyancy flux is one of the sources of TKE production as seen in Eq. (F-5-6) and is reinforced by latent heat brought by condensation. It plays an important role for producing turbulence in cloud layer at the top of boundary layer.

In the Level 3 model, the fluxes solved as Eqs. (F-5-17), (F-5-18), (F-5-19) and (F-5-20) are also represented by down gradient form. These equations implies that the diffusion coefficients K_m and K_h can be written as

$$K_m = S_M q \ell, \quad (\text{F-5-25})$$

$$K_h = S_H q \ell, \quad (\text{F-5-26})$$

where

$$S_M = S_{M2.5} + S_M', \quad (\text{F-5-27})$$

$$S_H = S_{H2.5} + S_H'. \quad (\text{F-5-28})$$

Note that although S_M and S_H correspond to C in Eq. (F-5-2), they are not constants but variables unlike the first order scheme.

The correction terms S_M' and S_H' appeared in the Level 3 model are proportional to the difference from the equilibrium state, given by

$$S_M' = E_M \left(\frac{\ell}{q^2} \frac{g}{\theta_0} \right)^2 [\overline{\theta_v'^2} - \overline{\theta_{v,2.5}'^2}], \quad (\text{F-5-29})$$

$$S_H' = -\frac{E_M}{G_H} \left(\frac{\ell}{q^2} \frac{g}{\theta_0} \right)^2 [\overline{\theta_v'^2} - \overline{\theta_{v,2.5}'^2}], \quad (\text{F-5-30})$$

where θ_v is the virtual potential temperature, of which self-correlation $\overline{\theta_v'^2}$ can be written with the

prognostic variables as

$$\overline{\theta_v'^2} = \beta_\theta \overline{\theta_1'^2} + 2\beta_\theta \beta_q \overline{\theta_1' q_w'} + \beta_q \overline{q_w'^2}, \quad (\text{F-5-31})$$

with the buoyancy parameters β_θ and β_q . E_M and E_H are again functions of G_M and G_H (for the full expressions, see Nakanishi and Niino (2004)), and subscript “2.5” denotes the value derived by the level 2.5 model. As $\overline{\theta_v'^2}$ is diagnosed in the level 2.5 model assuming that the local balance between the production and the dissipation of the TKE related variables, the value with the subscript “2.5” denote the one in the equilibrium state. Alternatively, it is often convenient to introduce Γ_θ and Γ_q such as Eq. (F-5-19) and (F-5-20) because they have simple forms given as

$$\Gamma_\theta \equiv S_H \left[\frac{\partial \overline{\theta_1'}}{\partial z} \right] = E_H \frac{1}{q^2} \frac{g}{\theta_0} [\overline{\theta_1' \theta_v'} - \overline{\theta_1' \theta_{v,2.5}'}], \quad (\text{F-5-32})$$

$$\Gamma_q \equiv S_H \left[\frac{\partial \overline{q_w'}}{\partial z} \right] = E_H \frac{1}{q^2} \frac{g}{\theta_0} [\overline{q_w' \theta_v'} - \overline{q_w' \theta_{v,2.5}'}], \quad (\text{F-5-33})$$

where

$$\overline{\theta_1' \theta_v'} = \beta_\theta \overline{\theta_1'^2} + \beta_q \overline{\theta_1' q_w'}, \quad (\text{F-5-34})$$

$$\overline{q_w' \theta_v'} = \beta_\theta \overline{\theta_1' q_w'} + \beta_q \overline{q_w'^2}. \quad (\text{F-5-35})$$

The correction induced by the level 3 appears when there is difference from the balanced state and variables such as $\overline{\theta_v'^2}$, $\overline{\theta_1' \theta_v'}$ and $\overline{q_w' \theta_v'}$, which are formed by the prognostic variable $\overline{\theta_1'^2}$, $\overline{q_w'^2}$ and $\overline{\theta_1' q_w'}$, have tendency of increasing or decreasing toward the equilibrium state. The correction terms can be regraded as counter gradient terms.

At the end of the previous section, importance of introducing the non-local effects was described. In the Level 3 model, while the counter gradients terms are induced, the form of the fluxes, seen in Eqs. (F-5-17), (F-5-18), (F-5-19) and (F-5-20), is still the down gradient one like the eddy viscosity model. However, it is revealed by experiments with the single column model that the Mellor-Yamada Level 2.5 and 3 (with the improvement described later) generate more uniform and more realistic mixed layer than the eddy viscosity model. Although the Level 2.5 model also has just only one prognostic variable, TKE, and no counter gradient terms or no non-gradient terms as well as the eddy diffusive model, the Level 2.5 model can realize better uniform mixed layer than the eddy diffusive model. It implies that more flexible diffusion coefficients due to the variable S_M and S_H help to generate more uniform layer than the eddy viscosity model in which C in Eq. (F-5-2) is constant. Moreover, the counter gradient term appeared in the Level 3 model gets the mixed layer slightly more uniform than without that. They imply that the more flexible diffusion coefficients and counter gradient term play the similar role to the non-local terms in the first order schemes despite that no non-local quantities are directly used.

F-5-3. Partial condensation and evaluation of buoyancy fluxes

As mentioned above, the buoyancy flux is strongly related to representation of cloud layer at the top of boundary layer, such as stratocumulus. Here, the method of how to evaluate the buoyancy flux will be demonstrated. Through this calculation, we can also obtain the cloud fraction and condensed water content. They are used in the radiation scheme to evaluate influences for shortwave and longwave radiation by clouds.

The buoyancy flux $\overline{w'b}$ is defined as

$$\overline{w'b} = \frac{g}{\theta_v} \overline{w'\theta_v'}, \quad (\text{F-5-36})$$

and is included in production term of TKE. Virtual potential temperature θ_v can be written with the conserved quantities as

$$\theta_v = \theta(1 + 0.61q_v - q_1) = \left(\theta_1 + \frac{\theta}{T} \frac{L}{C_p} q_1 \right) (1 + 0.61q_w - 1.61q_1), \quad (\text{F-5-37})$$

Therefore, $\overline{w'\theta_v'}$ becomes

$$\begin{aligned} \overline{w'\theta_v'} &= (1 + 0.61q_w - 1.61q_1) \overline{w'\theta_1'} + 0.61\theta \overline{w'q_w'} \\ &+ \left[\frac{\theta}{T} \frac{L}{C_p} (1 + 0.61q_w - 1.61q_1) - 1.61\theta \right] \overline{w'q_1'}. \end{aligned} \quad (\text{F-5-38})$$

The problem left is how to represent the condensed water flux $\overline{w'q_1'}$. In saturated cloudy air, the flux can be given with the Clausius-Clapeyron equation by

$$\overline{w'q_1'} = a \overline{w'q_w'} - b \overline{w'\theta_1'}, \quad (\text{F-5-39})$$

where

$$a = \left(1 + \frac{L}{C_p} q_{sl,T} \right)^{-1}, \quad b = a \frac{T}{\theta} q_{sl,T}, \quad q_{sl,T} = \frac{\partial q_{sl}}{\partial T}. \quad (\text{F-5-40})$$

In order to determine $\overline{w'q_1'}$ in partially cloudy air, it is one way and widely used to average the unsaturated and saturated ones with weight of cloud fraction R , which means

$$\overline{w'q_1'} = R(a \overline{w'q_w'} - b \overline{w'\theta_1'}). \quad (\text{F-5-41})$$

As a result, the buoyancy flux can be written only with $\overline{w'q_w'}$ and $\overline{w'\theta_1'}$ as

$$\overline{w'\theta_v'} = \beta_\theta \overline{w'\theta_1'} + \beta_q \overline{w'q_w'}, \quad (\text{F-5-42})$$

with

$$\beta_\theta = 1 + 0.61q_w - 1.61q_1 - Rbc, \quad (\text{F-5-43})$$

$$\beta_q = 0.61\theta + Rab, \quad (\text{F-5-44})$$

$$c = \frac{\theta}{T} \frac{L}{C_p} (1 + 0.61q_w - 1.61q_1) - 1.61\theta. \quad (\text{F-5-45})$$

Although the form of $\overline{w'\theta'_v}$ can be obtained, the cloud fraction R and condensed water content q_1 are still left undetermined and they should be set with other methods. Sommeria and Deardorff (1977) suggested one way to determine them assuming that the subgrid fluctuations of cloud water q_w and liquid water potential temperature θ_1 from their mean values obey the probability distribution represented by the bi-normal distribution function

$$G(\theta_1, q_w) = \frac{1}{2\pi\sigma_{\theta_1}\sigma_{q_w}\sqrt{1-r^2}} \exp\left[-\frac{1}{2(1-r^2)}\left(\frac{\theta_1'^2}{\sigma_{\theta_1}^2} - \frac{2r\theta_1'q_w'}{\sigma_{\theta_1}\sigma_{q_w}} + \frac{q_w'^2}{\sigma_{q_w}^2}\right)\right], \quad (\text{F-5-46})$$

where

$$\sigma_{\theta_1}^2 = \overline{\theta_1'^2}, \quad \sigma_{q_w}^2 = \overline{q_w'^2}, \quad r = \frac{\overline{q_w'\theta_1'}}{\sigma_{\theta_1}\sigma_{q_w}}. \quad (\text{F-5-47})$$

Under this assumption, the cloud fraction R and the condensed cloud water content $\overline{q_1}$ can be obtained as moments of the distribution such as

$$R = \int_{-\infty}^{\infty} d\theta_1 \int_{q_s}^{\infty} dq_w G(\theta_1, q_w) = \frac{1}{2} \left[1 + \operatorname{erf}\left(\frac{Q_1}{\sqrt{2}}\right) \right], \quad (\text{F-5-48})$$

$$\overline{q_1} = \int_{-\infty}^{\infty} d\theta_1 \int_{q_s}^{\infty} dq_w (q_w - q_s) G(\theta_1, q_w) = 2\sigma_s \left(RQ_1 + \frac{1}{\sqrt{2\pi}} \exp\left[-\frac{Q_1^2}{2}\right] \right), \quad (\text{F-5-49})$$

where

$$\sigma_s^2 \equiv \frac{1}{4} \left(a^2 \overline{q_w'^2} - 2ab \overline{q_w'\theta_1'} + b^2 \overline{\theta_1'^2} \right), \quad (\text{F-5-50})$$

$$Q_1 \equiv \frac{a\Delta\overline{q}}{2\sigma_s}, \quad (\text{F-5-51})$$

$$\Delta\overline{q} \equiv \overline{q_w} - \overline{q_{sl}}, \quad (\text{F-5-52})$$

$$a = \left[1 + \frac{L}{C_p} \left(\frac{\partial q_s}{\partial T} \right)_{T=\overline{T_1}} \right]^{-1}, \quad b = a\Pi \left(\frac{\partial q_s}{\partial T} \right)_{T=\overline{T_1}}, \quad (\text{F-5-53})$$

$\overline{q_{sl}}$ is the saturated specific ratio of vapour at $\overline{T_1} \equiv \overline{T} - \frac{L}{C_p} q_1$, and erf means the error function

$$\text{erf}(x) = \frac{2}{\sqrt{\pi}} \int_0^x e^{-u^2} du. \quad (\text{F-5-54})$$

Mellor and Yamada (1982) took a slightly different way to determine $\overline{w'q_1'}$ in partially cloudy air from what is mentioned above. They derived the relation

$$\frac{\overline{\phi'q_1}}{a\overline{\phi'q_w} - b\overline{\phi'\theta_1}} = R' \equiv R - \frac{q_1}{2\sigma_s} \frac{1}{\sqrt{2\pi}} \exp\left(-\frac{Q_1^2}{2}\right), \quad (\text{F-5-55})$$

by integrating

$$\overline{\phi'q_1} = \int_{-\infty}^{\infty} d\theta_1 \int_{q_s}^{\infty} dq_w \phi q_1 G(\theta_1, q_w), \quad (\text{F-5-56})$$

for $\phi = \theta_1$ or q_w , and assumed that this relation might be valid also for $\phi = w$ by considering the tri-normal distribution function. In this way, they obtained

$$\overline{w'q_1} = \tilde{R}(a\overline{w'q_w} - b\overline{w'\theta_1}). \quad (\text{F-5-57})$$

The difference from the former one is using \tilde{R} instead of R . At the limit of the fully saturated situation ($Q_1 \rightarrow \infty$) and the cloud free one ($Q_1 \rightarrow -\infty$), the difference between them is vanished. In NHM, the formulation by Mellor-Yamada (1982) has been adopted.

The cloud fraction R and the cloud water content q_1 are given as the function of the total water $\overline{q_w}$ on each grid for a fixed σ_s . One can find from Eqs. (F-5-48) and (F-5-49) that even in the unsaturated state ($\Delta\overline{q} < 0$), R and $\overline{q_1}$ can be non-zero. Especially for a larger σ_s , R and $\overline{q_1}$ can be relatively large even when $\overline{q_w}$ is much less than $\overline{q_{sl}}$. Note that at the saturated point ($\Delta\overline{q} = 0$), R is always 0.5 no matter how large σ_s is.

The cloud fraction and condensed water content are evaluated on the basis of turbulence fluctuation. This formulation has been confirmed valid for stratocumulus where Q_1 is significantly large in terms of the buoyancy flux, although not suitable for convective clouds where Q_1 is often negative and the distribution is positively skewed (e.g. Bougeault(1981)). As a result, cloud fraction evaluated by the scheme was too small, leading to excessive shortwave radiation flux towards surface since the cloud fraction and condensed water content are used in the radiation process. In order to solve the issue, when cloud fraction and condensed water content are calculated for those used in the radiation scheme, the lower limit for σ_s has been implemented such as

$$f_{\min} a \cdot r \cdot q_{sl} < \sigma_s, \quad (\text{F-5-58})$$

where r is the factor which is 1 above 850hPa, decreasing linearly on pressure to 0 at the surface, to reduce excessive cloud generation near the surface for unsaturated status, and f_{\min} is a parameter to be tuned. A larger f_{\min} could compensate the shortage of cloud distribution because large σ_s can bring wider cloud distribution. (Note that this limit is not applied to evaluate the buoyancy flux.) Finally, we chose the value 0.09 as the value of f_{\min} so that bias of shortwave radiation flux towards surface and screen level temperature can be effectively reduced. While the previous scheme to

evaluate cloud fraction based on a function of relative humidity tended to give too much cloud distribution and lead to significantly large negative bias of shortwave radiation flux towards surface, the new cloud fraction reduces the negative bias considerably well and raise accuracy of the screen temperature at 1.5m.

F-5-4. Improvement in the Mellor-Yamada model by Nakanishi and Niino

Nakanishi (2001), Nakanishi and Niino (2004, 2006) (hereafter, NN) made several improvements in the original Mellor-Yamada model from the view of amending closure constants and being more stabilized. The Mellor-Yamada model contains several closure constants and the mixing length which should be determined by experiments such as observations and numerical simulations with higher resolutions. NN conducted some LES simulations and revised the closure constants and the mixing length referring to their LES results. NN's revises include activating buoyancy- and shear- related terms which are neglected in the original one.

In the improved model (called MYNN), the mixing length are also revised on the basis of their results by LES, given by

$$\frac{1}{\ell} = \frac{1}{L_S} + \frac{1}{L_T} + \frac{1}{L_B} \quad (\text{F-5-59})$$

where

$$L_S = \begin{cases} kz/3.7 & (\zeta \leq 1) \\ kz(1 + 2.7\zeta)^{-1} & (0 \leq \zeta < 1) \\ kz(1 - \alpha_4\zeta)^{0.2} & (\zeta < 0) \end{cases} \quad (\text{F-5-60})$$

$$L_T = \alpha_1 \frac{\int_0^\infty qz \, dz}{\int_0^\infty q \, dz} \quad (\text{F-5-61})$$

$$L_B = \begin{cases} \alpha_2 q / N_1 & (\partial\theta/\partial z > 0, \zeta \geq 0) \\ [\alpha_2 q + \alpha_3 (q_c / L_T N_1)^{1/2}] / N_1 & (\partial\theta/\partial z > 0, \zeta < 0) \\ \infty & (\partial\theta/\partial z < 0) \end{cases} \quad (\text{F-5-62})$$

with the Brunt-Väisälä frequency N_1 , empirical constants α_1 , α_2 , α_3 and α_4 set to be

$$(\alpha_1, \alpha_2, \alpha_3, \alpha_4) = (0.23, 1.0, 5.0, 100.0), \quad (\text{F-5-63})$$

and $\zeta = z / L$ with the Monin-Obukhov length L .

The differences from the original one are that

1. the parameter representing the stability at surface is included in L_S so that L_S can be larger above unstable surface layer and smaller above stable one.
2. the effect brought by buoyancy is introduced depending on the Brunt-Väisälä frequency. The similar term was introduced by the model by Deardorff (1980) as Eq. (F-5-4)

The comparison between the original mixing length and the revised one shows that momentum and heat staying at the lower layer with the original one can be more transported upwards with the revised one. It is thought to be brought by the revision of L_s including the contributions of the stability at surface layer.

Furthermore, the original Mellor-Yamada model more than level 2.5 is known to having some singularities. Helfand and Labraga (1988) analysed the pathological behaviour in the level 2.5 model when TKE is increasing, that is, $q^2 < q_e^2$ where q_e^2 is TKE in the equilibrium state. In order to remove the singularity, they suggested the modifications that $S_{M2.5}$ and $S_{M2.5}$ should be replaced with $S_{M2} \times q / q_e$ and $S_{H2} \times q / q_e$, respectively. NN expanded their discussion to the level 3 model and incorporated additional modifications depending on the relation between $\overline{\theta_1}$ in the level 3 and 2.5 models.